GENERAL APPLIED SCIENCE LABORATORIES, INC.



# THIRD QUARTERLY PROGRESS REPORT

## CONTRACT NASW-2235

GASL Job 5865

Period: January 15, 1972 - April 15, 1972

Prepared for

Lewis Research Laboratories
National Aeronautics and Space Administration
Cleveland, Ohio

Prepared by

General Applied Science Laboratories, Inc.
Merrick and Stewart Avenues
Westbury, New York 11590

Third Quarterly Progress Report

Contract NASW-2235

GASL Job 5865

Period: January 15, 1972 - April 15, 1972

# RESEARCH ON TURBOJET COMBUSTOR POLLUTANT FORMATION

## I. INTRODUCTION

The goal of this research is to develop a modular computer program for the description of gas-turbine combustor flow and chemical fields. The model will predict combustion efficiency and pollutant formation and disposition.

The model is being developed with recognition of the extreme importance of the coupling between fluid-dynamical and chemical-kinetic mechanisms. Turbulent mixing and detailed kinetics processes for the broad division of the model within which the effects of swirl, recirculation, droplet evaporation and combustion, and coupled oxidation/$NO_x$ formation mechanisms are included.

Because of the complexity of the turbojet combustor flow and chemical fields, the model is being developed via a systematic unit-problem-approach wherein each mechanism is quantified in modular form. Coupling of all the relevant mechanisms will yield a unified model having the property of being able to isolate each process. This feature is regarded as important in terms of updating and extending aspects of the model that rely upon empirical information for definition. For example, turbulent-exchange coefficients and kinetic-rate constants fall into this category. An additional advantage of the modular development approach is that during the construction of the unified model each unit analysis may be independently applied for parametric studies to aid in evaluating the relative importance of each mechanism over ranges of operating conditions of interest in turbojet combustors.

This report presents the status of added development made during this quarter to three (3) key elements of the unified model: Turbulent mixing with swirl, turbulent mixing with swirl including finite-rate kinetics, and multiphase recirulation zone analysis. Each of these key elements will be discussed in some detail in the sections to follow. However, the following is a capsule review of some of the results so far with regard to these key elements of the unified model:

Turbulent Mixing With Swirl -

- Theoretical comparisons with experiments involving small, moderate and large degrees of swirl is quite good.

- For cases involving small and moderate degrees of swirl adequate representation of the resulting flow field can be obtained by assuming that the turbulent transport terms are functions of the axial coordinate only.

- For large degrees of swirl closer agreement with experimental data is obtained by assuming the turbulent diffusion terms to be dependent upon radial as well as the axial direction.

- The solution technique is capable of treating ducted as well as free jet flows.

Multiphase Recirculation Zone Analysis (Effects of Water Injection on $NO_x$ Formation) -

- Theoretical comparisons with experiments relating the effects of water injection in the $NO_x$ reduction are quite encouraging.

- Parametric studies made to date on the effects of water-droplet size and state indicate that significantly less reduction in $NO_x$ is produced the larger the droplet size for a given residence time.

- For a given droplet diameter and water-to-fuel mass fraction increasing the residence time increases the % reduction in NO, however, with a concomitant increase in NO level.

- Under the specific conditions for which the parametric tests were made, injection of 10 $\mu$ water droplets gave rise to percent reductions in NO which were insensitive to residence time.

Turbulent Mixing with Swirl (Including Finite Rate Kinetics) -

- A computer program which includes all the options built into the nonreacting turbulent mixing analysis (with swirl) together with the quasi-global finite rate kinetics analysis has been developed and is in the so-called "debugging" stage.

## II. STATUS OF MODEL DEVELOPMENT

During this quarterly period, applications of the sub-models for mixing with swirl and multiphase recirculation zones were extended to investigate flows with large degrees of swirl and to study the effects of water injection on the reduction in $NO_x$ formation. When applicable, comparisons between theory and experiments are made. In addition, work initiated during the last quarter involving the coupled mixing and kinetics program including swirl has resulted in a computer program which is currently in the "debugging" stage. Also, the recirculation zone analysis involving detailed methane kinetics is in the process of being made operational.

### A. Mixing and Swirl

Experimental studies on swirl jets have shown that mixing can be substantially increased by imparting a swirling motion to the jet. The presence of the tangential velocity results in radial and axial pressure gradients that, in the case of strong swirl, result in reverse flow along the axis. Combustion studies, References (1), (2), (3) and (4), with free and confined swirling flames have shown that flames are reduced in length and increased in width as a result of swirl. In addition, stability was improved and combustion intensity increased as a result of swirl. Thus, since swirl, commonly employed in turbine combustors, offers a means for controlling mixing rates, residence times, and flame stabilization, all of which are factors tantamount to the possible control of pollutant emissions, a mathematical model has been developed which accounts for some of the effects of swirl.

The requisite analysis and some experimental results have already been discussed in Reference 5. However, for completeness the finite difference form of the governing equations are again presented in Appendix A. Some additional comparisons between the experiments of Reference 6 with the analysis have been made during this quarter of effort. The data has been generated from experiments classified as those exhibiting a large degree of swirl. Figures (1) through (8) show the comparative agreement for this set of experiments with the analysis. Judging by the complexity of the flow and by the difficulty in extracting the data, the overall agreement is quite good. Accordingly, the comparative agreement

presented here taken together with that depicted in the past quarterly (Reference 5) indicates that the analysis is quite adequate in predicting the fluid mechanical behavior for a broad spectrum of swirling flows and that this analysis can now be linked to an appropriate kinetics scheme for the purpose of studying combustion within swirling flows. Noteworthy also is that the theoretical results depicted in Figures (1) through (8) have been obtained by utilizing a turbulent eddy transport model that is both radially and axially dependent. This model, described in more detail in Reference (7), was devised by examining the axial velocity profile histories for several degrees of swirl as typified in Figure 9 as well as the findings of Reference (8) where it is shown that the nonisotropic character of turbulent stress distribution increases with increasing swirl. The results of our theoretical efforts in attempting to establish closer agreement between theory and experiment also imply that the turbulent transport process is strongly dependent upon the change in the character of the flow as the level of swirl increases. Figure 9 shows a probable reason for this behavior where for the large swirl the axial velocity profiles in the near-jet region exhibit velocity maxima off the jet axis. Accordingly, from a mixing lenth concept it appears that two length scales are appropriate in describing the eddy transport across the jet within this region. In fact as it is pointed out in Reference (8), the regions of maximum shear stress correspond to regions of maximum radial gradients of axial velocity. Consequently, it appears that associating a different level of eddy viscosity for each region of the jet profile that is separated by the point where the velocity is a maximum is valid on physical grounds. That <u>at least</u> two mixing lengths scales are appropriate in describing the turbulent eddy diffusivity in the near jet region is further substantiated by examining Figure 10 taken from Ref. 9. In this figure the radial distribution of turbulent kinetic energy is plotted at four downstream stations. These data were obtained from hot wire measurements and depict a peak in the turbulent kinetic energy profile in the near jet region (x/D = 1). Although one cannot directly correlate this data with that of Reference (8) or the axial velocity profile data of Figure 9, it does seem to appear that the location in the peak of turbulent kinetic energy follows closely with the location in the peak of axial velocity as well as the shift of both peaks towards the axis with increasing downstream distance. However, these observations are quite preliminary in nature and the study to date indicates that a further need for detailed analytical/expermental studies in turbulent swirling flows, particularly in assessing their transport properties is required.

B. Multiphase Recirculation Zone Analysis

For the treatment of flow regions involving intense back-mixing a stirred reactor analysis is used. The analysis has already been discussed, Reference (5), but the equations and solution technique are outlined in Apppendix B.

Recently substantial interest has been shown in the control of nitrogen oxide emissions from gas turbine engines using water injection, References (10) and (11). To date, however, there have not been any attempts to quantify the conditions under which water injection will be effective in the reduction of $NO_x$ emissions. What is of interest are such things including: droplet size, liquid vs vapor injection, the relative importance of kinetic modifications compared with thermal modifications, and the amount of water required to yield a significant reduction in $NO_x$.

The stirred reactor model is appropriate for such a study since it is within the primary zone, prior to dilution, where the NO is formed.

During this period a study was initiated to help establish the effect of water injection. The data of Reference 11 was compared with the theory as part of this study. The results are shown in Figures 11, 12 and 13 for a near-stoichiometric, adiabatic primary zone. Figure 11 shows the percent reduction in NO as a function of the water-to-fuel mass ratio for various initial water droplet diameters. Steam injection is also shown in Figure 11 and it should be noted that the water droplets were injected at 300°K whereas the steam was injected at 422°K. The residence time was about 3 msecs and remained essentially invariant with the amount of water (or steam) injected. The data shown was for different power settings and for both steam and liquid injection. Of interest is the agreement between theory and experiment for the 10 micron diameter water droplets. This size droplet was indicated in Reference 11 as being relevant to those experiments. Of further interest is the fact that the hotter steam produced essentially the same reduction in NO which is in direct agreement with the experimental observations. For the larger droplet sizes there is significantly less reduction in NO and this is associated with the reduced evaporation rate as the droplet size increases. It appears then that for these particular conditions the heat capacity of the water is more important than the latent heat of vaporization in terms of reducing peak temperatures. Figure 12 shows the effect of

residence time upon the percent reduction of NO. It must be kept in mind that the NO level increases with increased residence time. It is interesting to note, however, that for the smaller droplets (10 $\mu$) the percent reduction in NO is insensitive to residence time whereas for the larger droplets the effect of size is significant. This again is due to the evaporation rate decreasing with increased droplet size. Figure 13 shows the effect of residence time and water-to-fuel mass ratio on the reduction of NO as a function of initial droplet size. Here it is interesting to note that above about 10 $\mu$ diameter droplets the reduction in NO is greater for the longer residence times. Of course, the absolute levels of NO are greater for the longer residence times but the observed effect is related to the relative rate of evaporation compared with the rate of NO formation as the residence time increases. These results are indicative of the importance of droplet size. Although not shown here the effect of water injection upon CO levels is very small which is in agreement with the experimental observations, Reference 11.

## III. CURRENT PROBLEMS

During this period no special problems affecting the performance of the program have been encountered.

## IV. WORK PLANNED

During the next report period the coupled mixing and kinetics region including swirl will be debugged. Concurrently, the recirculation zone analysis with detailed methane kinetics will be made operational. Comparison of theory with data will be initiated.

## REFERENCES

1. Chigier, N.A., and Chervinsky, A., "Aerodynamic Study of Turbulent Burning Free Jets with Swirl," Eleventh Symposium (International) on Combustion, The Combustion Institute, 1967.

2. Beer, J. M., Combustion, 37, 27, 1965.

3. Niedzwiecki, R. W., Juhasz, A.J., and Anderson, D.N., "Performance of Swirl-Can Primary Combustor to Outlet Temperatures of 3600°F (2256°K)," NASA TM X-52902, 1970.

4. Niedzwiecki, R. W., Jones, R. E., "Combustion Stability of Single Swirl-Can Combustor Modules Using ASTM-A1 Liquid Fuel," NASA TN D-5436, October, 1969.

5. Second Quarterly Progress Report, Contract NASW-2235, by GASL, January 15, 1972.

6. Chigier, N.A. and Chervinsky, A., "Experimental Investigation of Swirling Vortex Motions in Jets," J.Appl. Mech., 34,1967.

7. Seventh Progress Report, Contract NASW-2235, by GASL, February 15, 1972.

8. Lilley, D.G. and Chigier, N.A., "Nonisotropic Exchange Coefficients in Turbulent Swirling Flames from Mean Value Distributions," Combustion and Flame, 16, 1971.

9. Pratte, B.D. and Keffer, J. F., "The Swirling Turbulent Jet," ASME Paper No. 72-FE-18.

10. Hilt, M. B. and Johnson, R. H., "Nitric Oxide Abatement in Heavy Duty Gas Turbine Combustors by Means of Aerodynamics and Water Injection," ASME Paper No. 72-GT-53, 1972.

11. Klapatch, R. D. and Koblish, T.R., "Nitrogren Oxide Control with Water Injection in Gas Turbines," ASME Paper No. 71-WA/GT-9, November 1971.

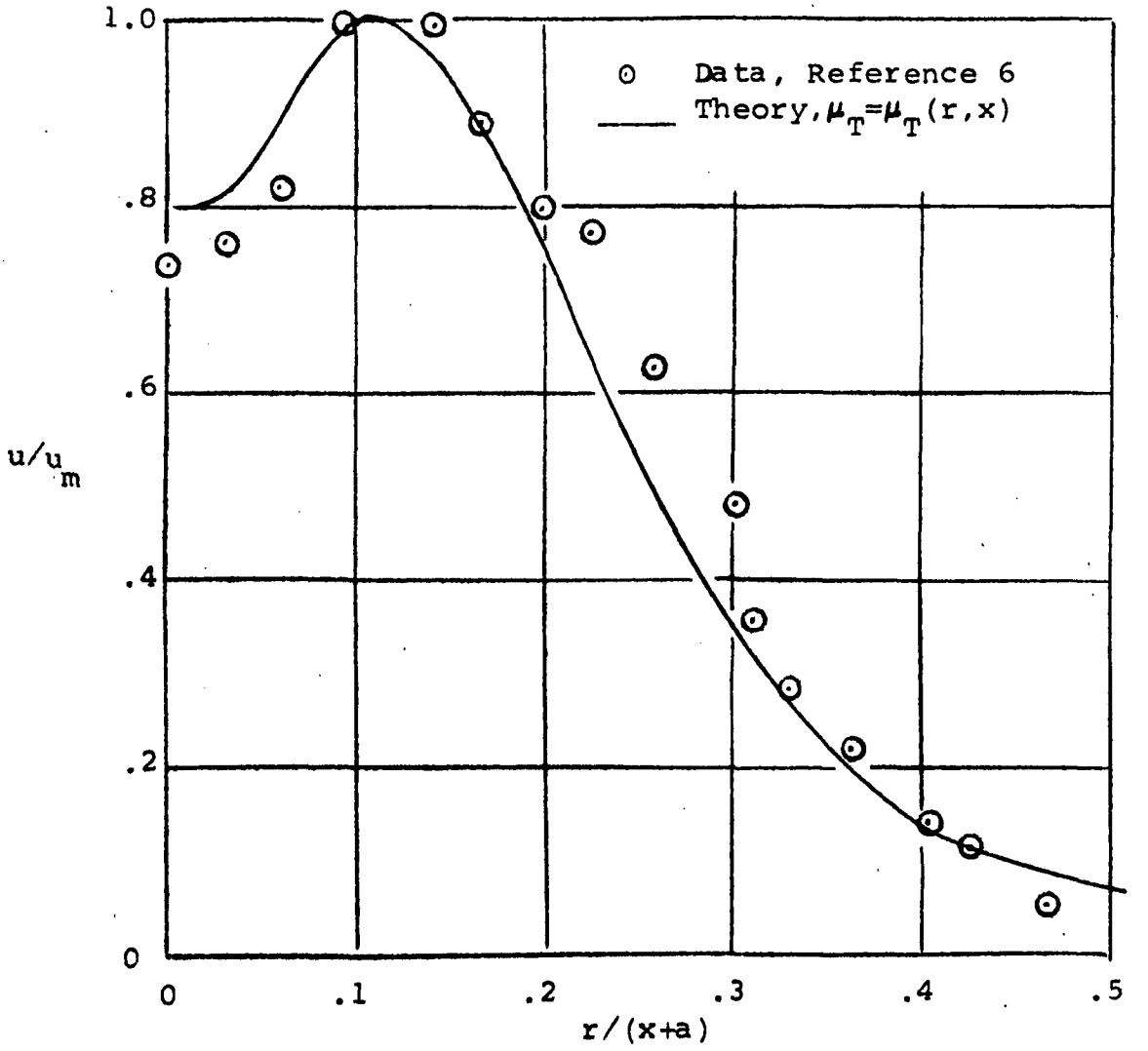


FIGURE 1 - COMPARISON, THEORY/EXPERIMENT, AXIAL VELOCITY
S = 0.6, x/D = 4.1

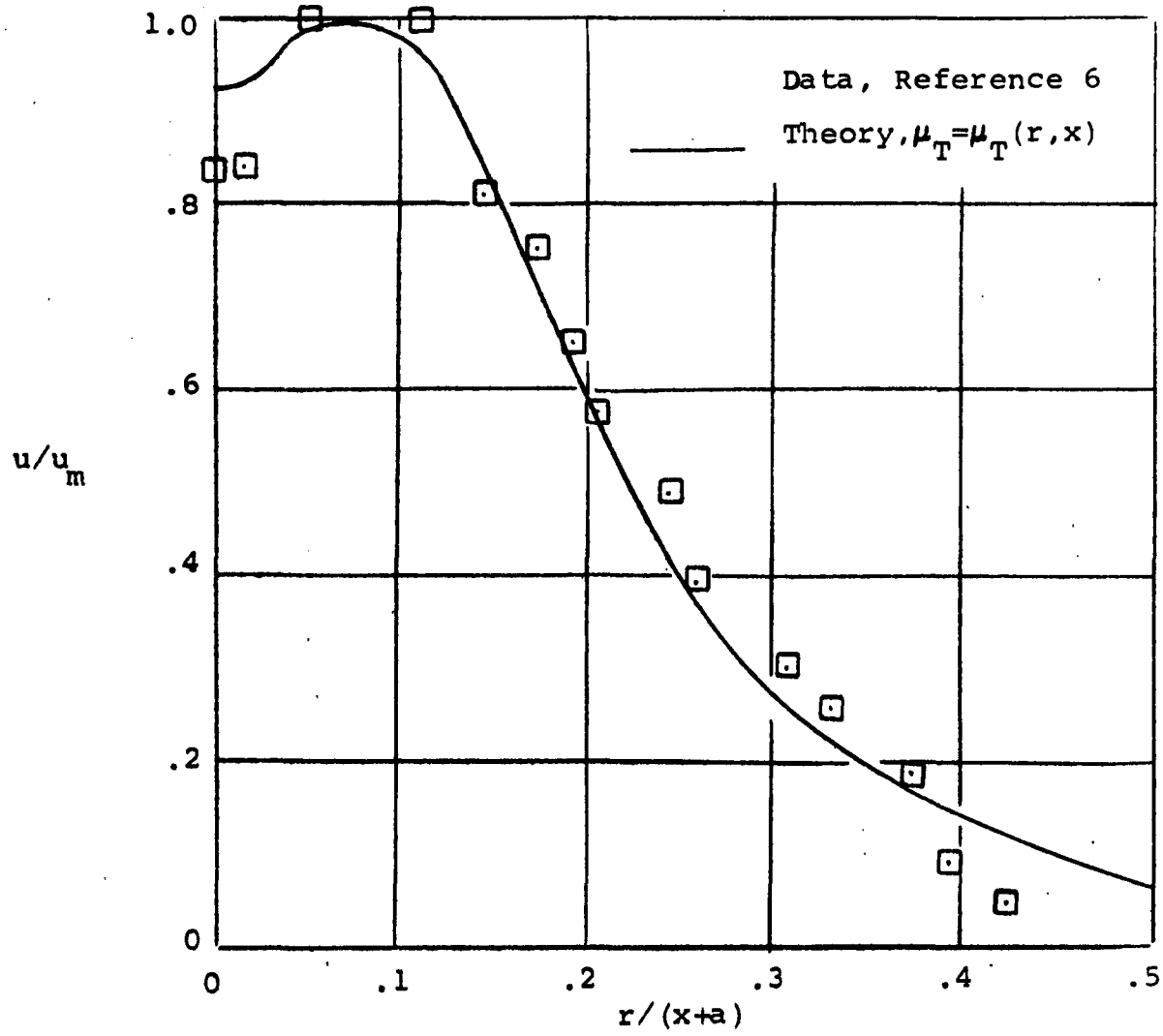


FIGURE 2 - COMPARISON, THEORY/EXPERIMENT, AXIAL VELOCITY
S = 0.6, x/D = 6.2

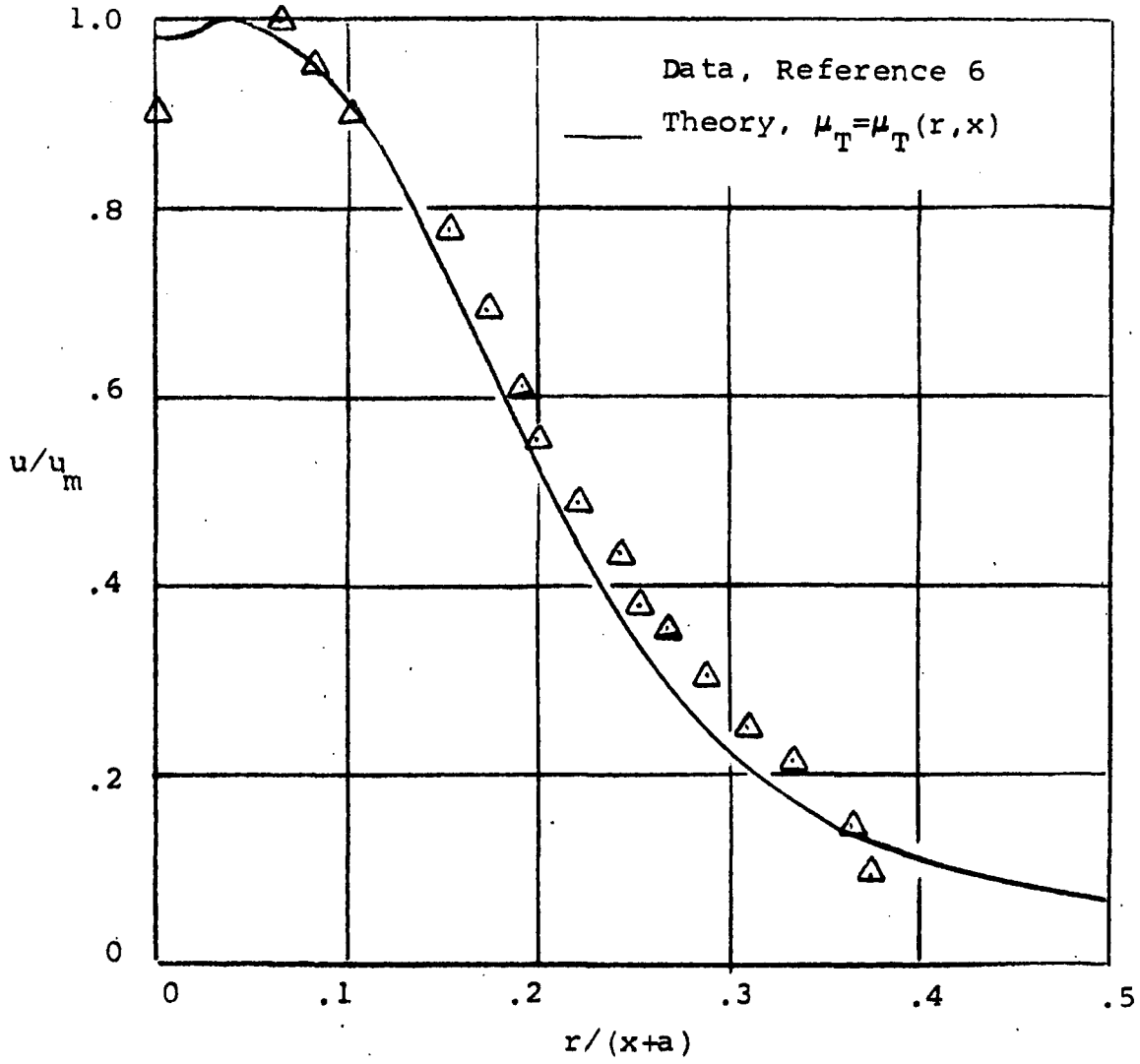


FIGURE 3 - COMPARISON, THEORY/EXPERIMENT, AXIAL VELOCITY
S = 0.6 , x/D = 8.3

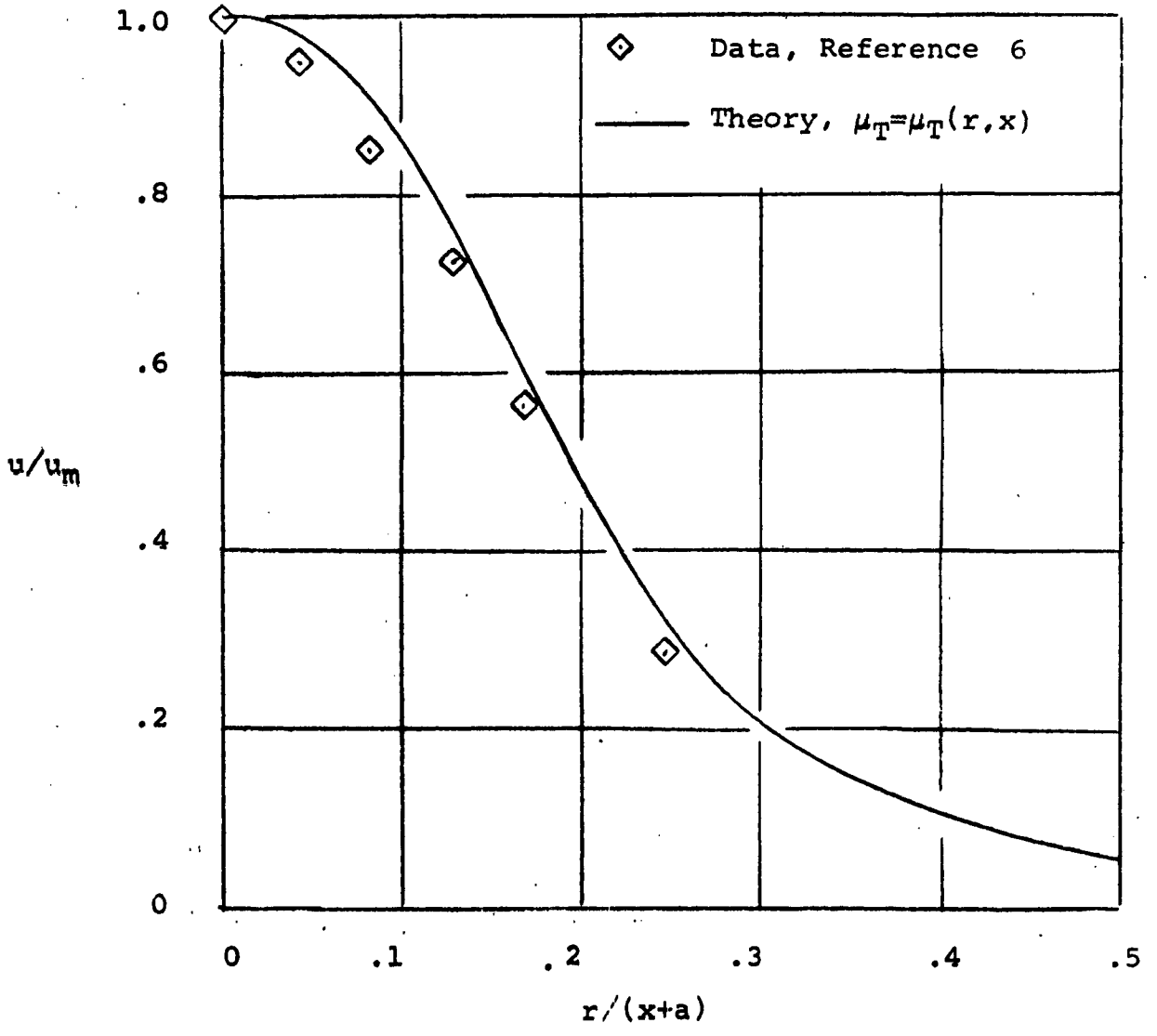


FIGURE 4 - COMPARISON, THEORY, EXPERIMENT, AXIAL VELOCITY

S = 0.6 , x/D = 10

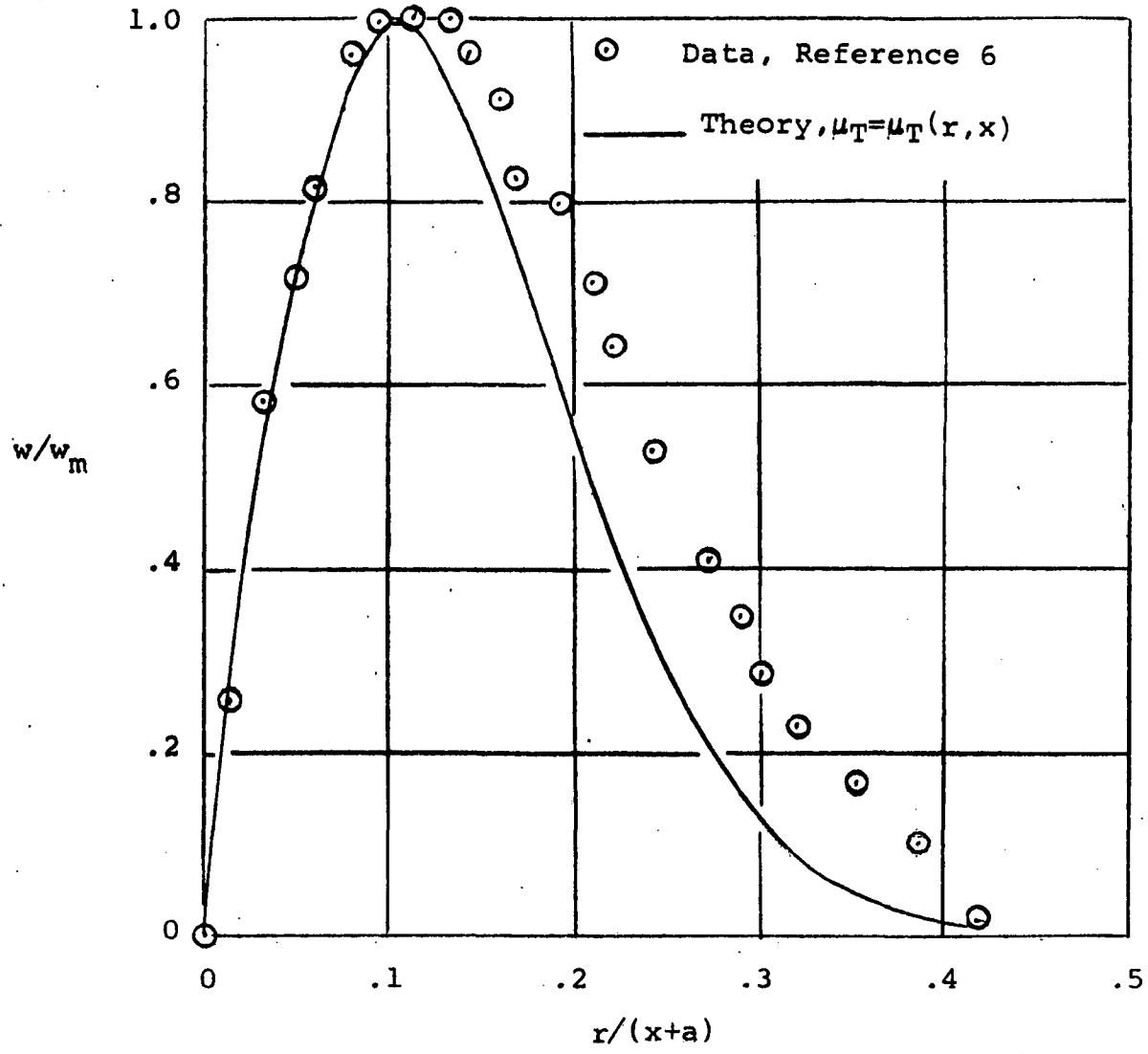


FIGURE 5 - COMPARISON, THEORY/EXPERIMENT, TANGENTIAL VELOCITY

S = 0.6 , x/D = 4.1

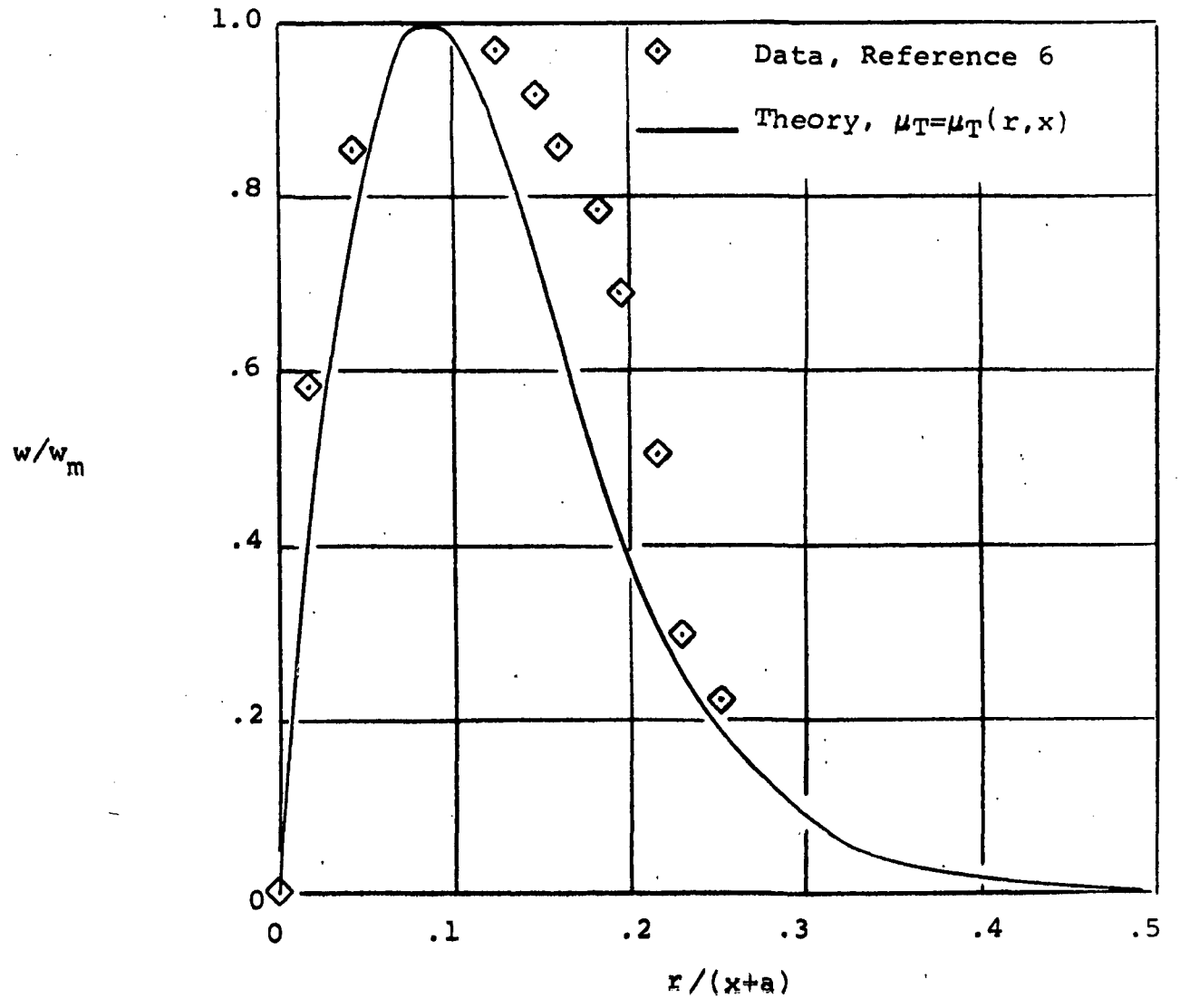


FIGURE 6 - COMPARISON, THEORY.EXPERIMENT, TANGENTIAL VELOCITY

S = 0.6 , x/D = 6.2

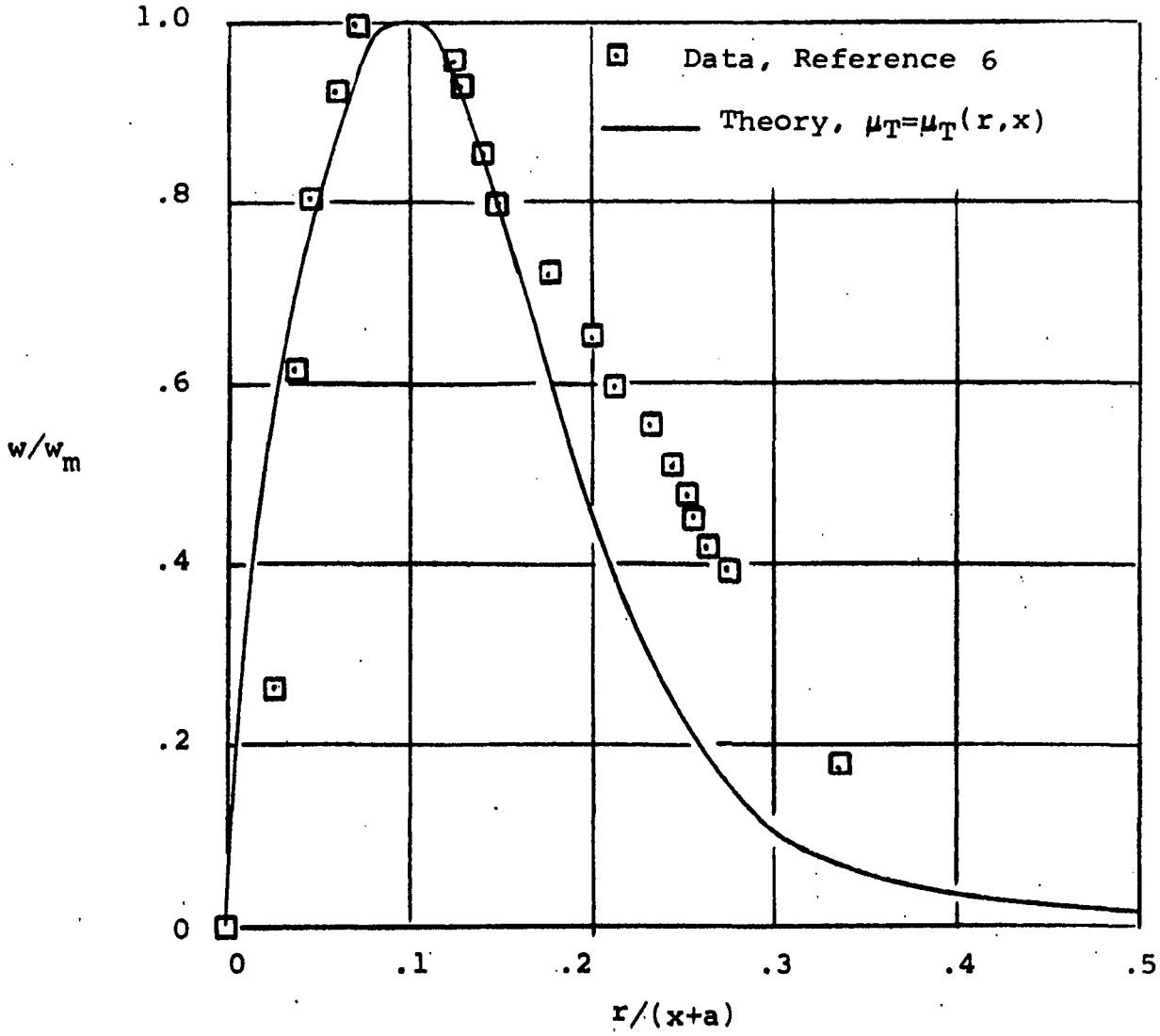


FIGURE 7 - COMPARISON, THEORY/EXPERIMENT, TANGENTIAL VELOCITY

S = 0.6 , x/D = 8.3

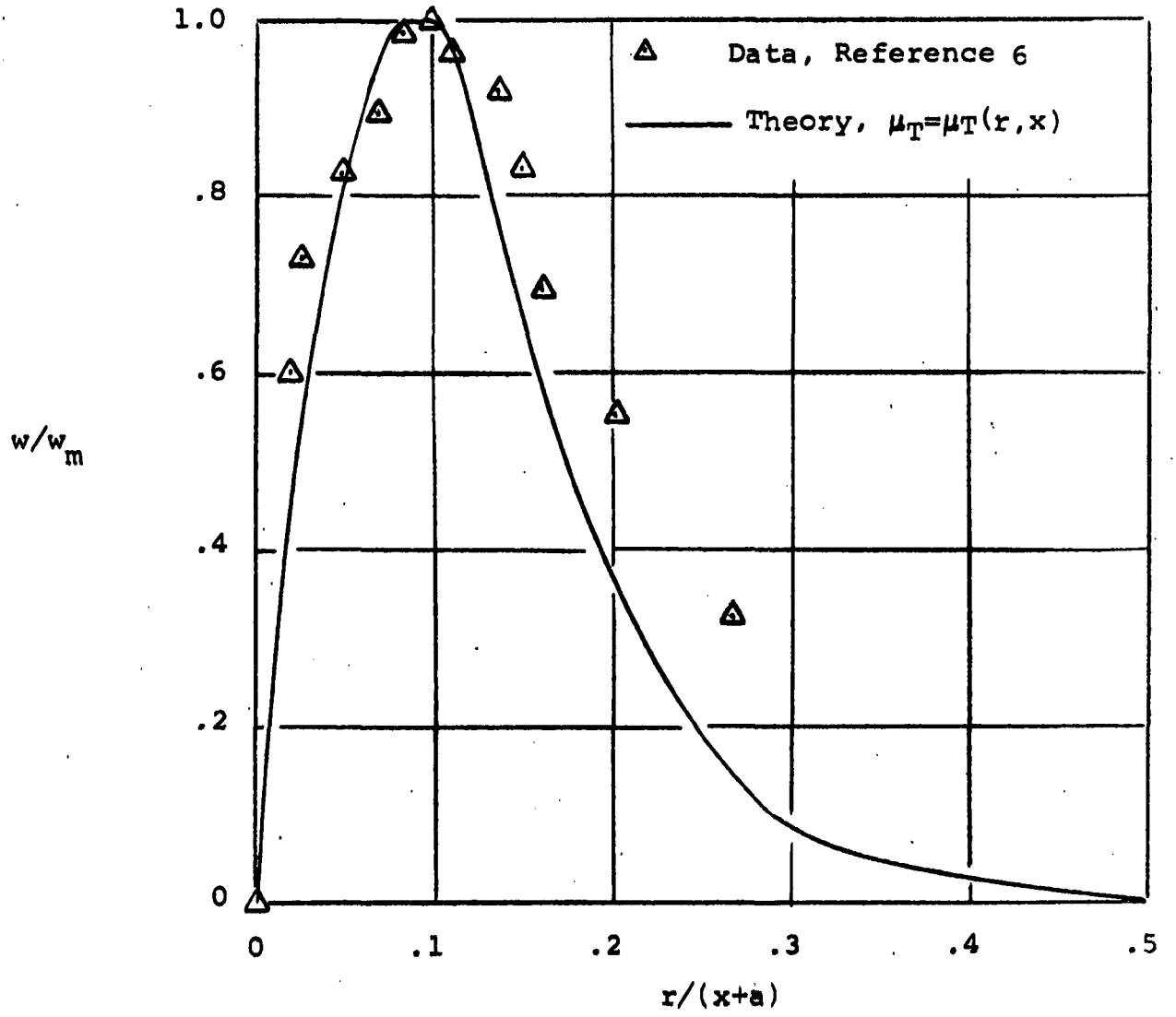


FIGURE 8 - COMPARISON, THEORY/EXPERIMENT, TANGENTIAL VELOCITY

S = 0.6 , x/D = 10.

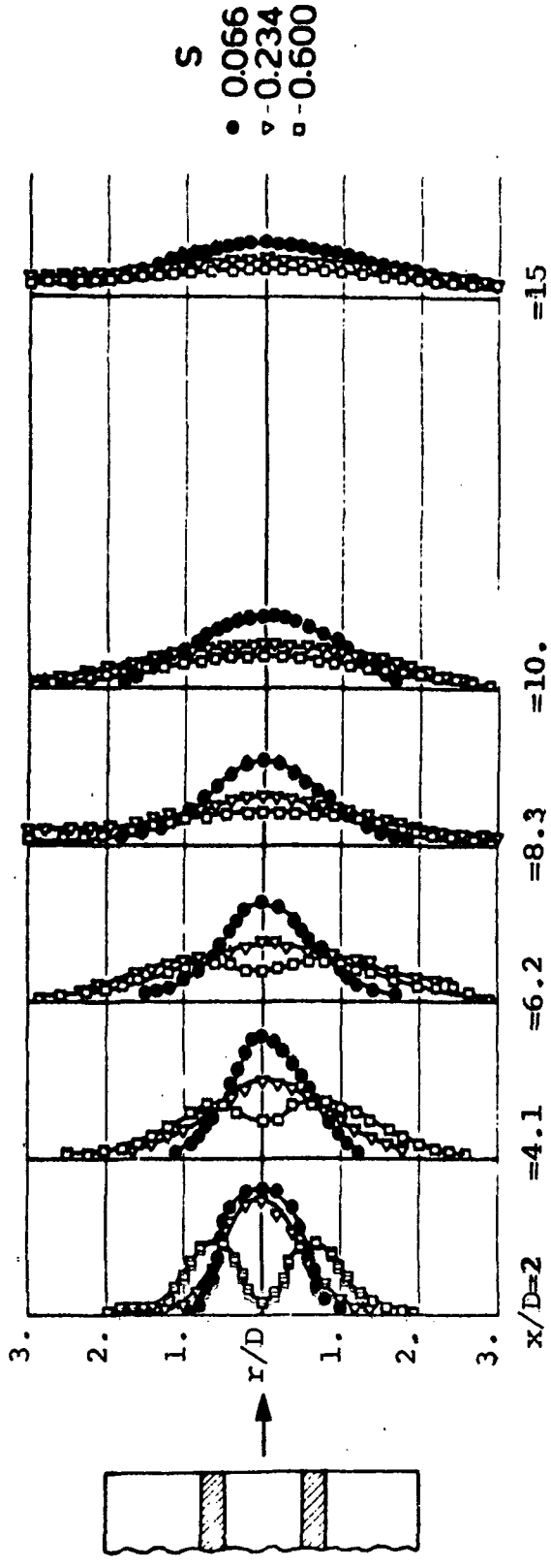


FIGURE 9 - RADIAL DISTRIBUTION OF VELOCITY VECTOR

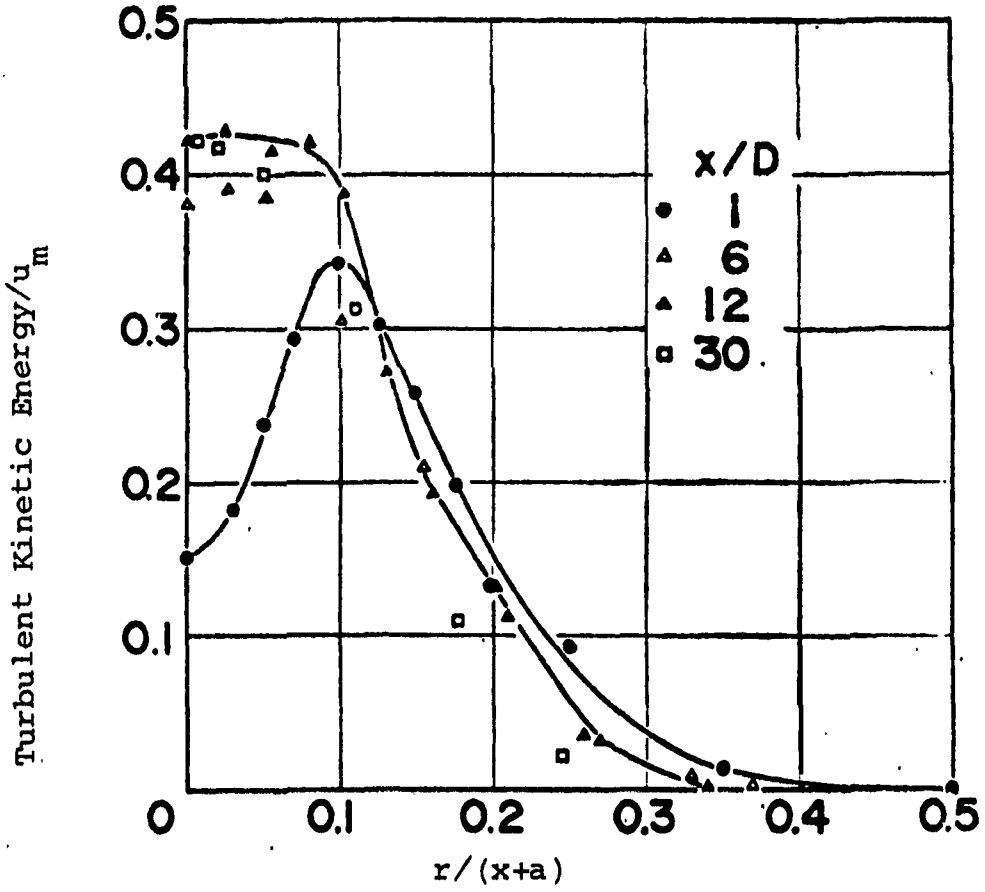


FIGURE 10 - TURBULENT KINETIC ENERGY DISTRIBUTION IN SWIRLING JET (REF. 9)

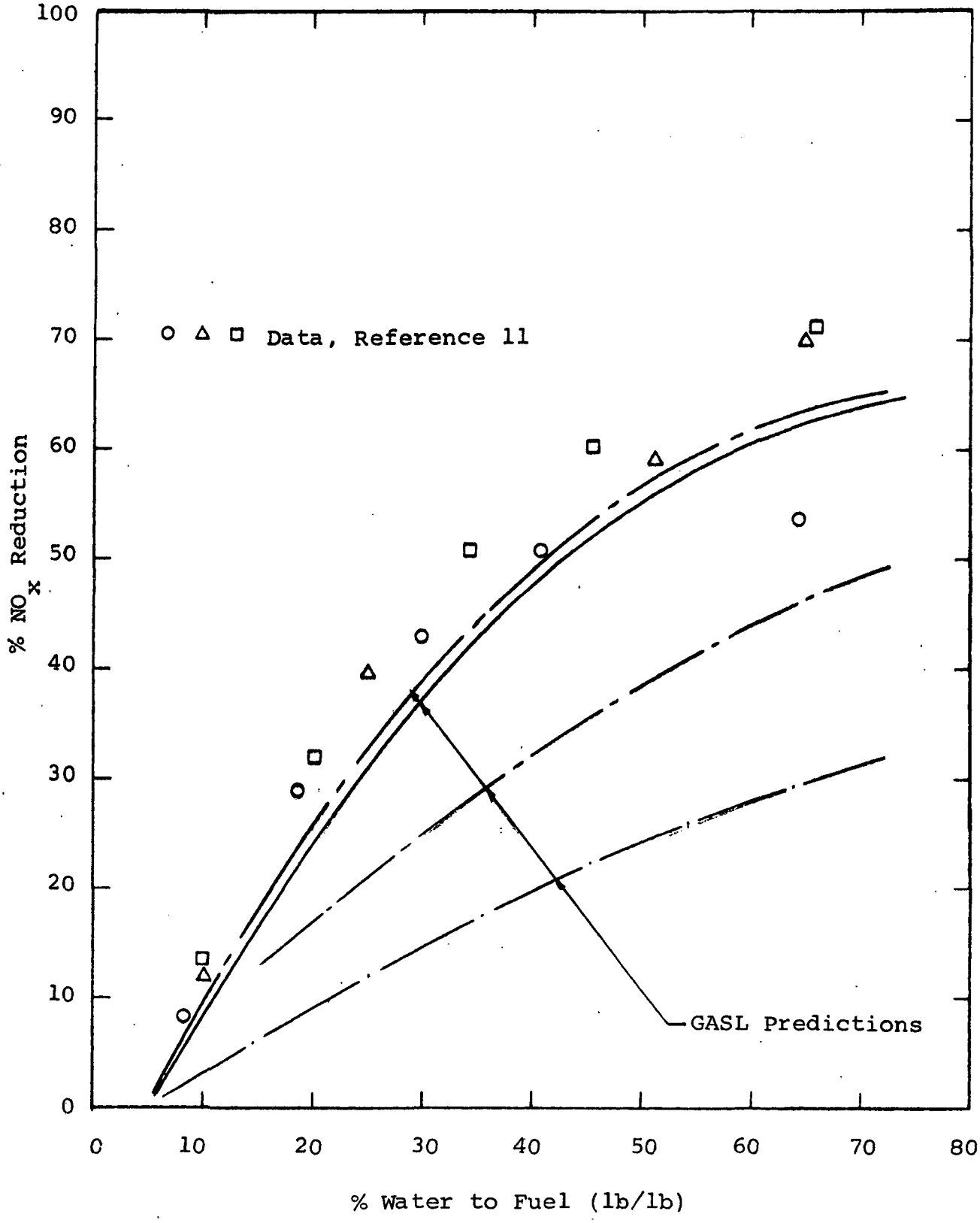


FIGURE 11 - COMPARISON, PRESENT THEORY/TURBINE COMBUSTOR DATA - EFFECT OF WATER AND STEAM INJECTION UPON $NO_x$ REDUCTION

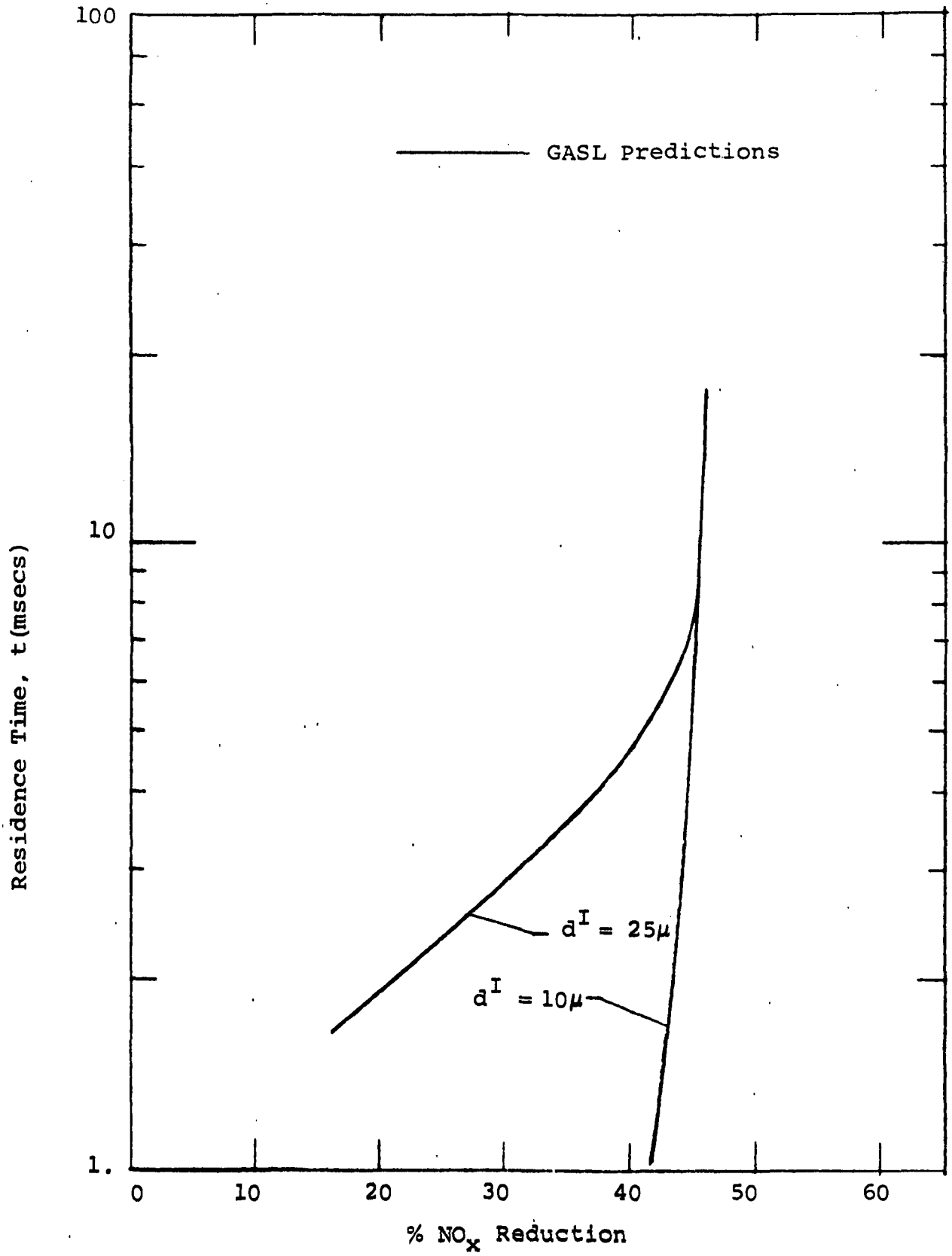


FIGURE 12 - RESIDENCE TIME vs NO REDUCTION AS A FUNCTION OF DROPLET SIZE, 40% WATER-TO-FUEL MASS RATIO, THEORETICAL PREDICTION

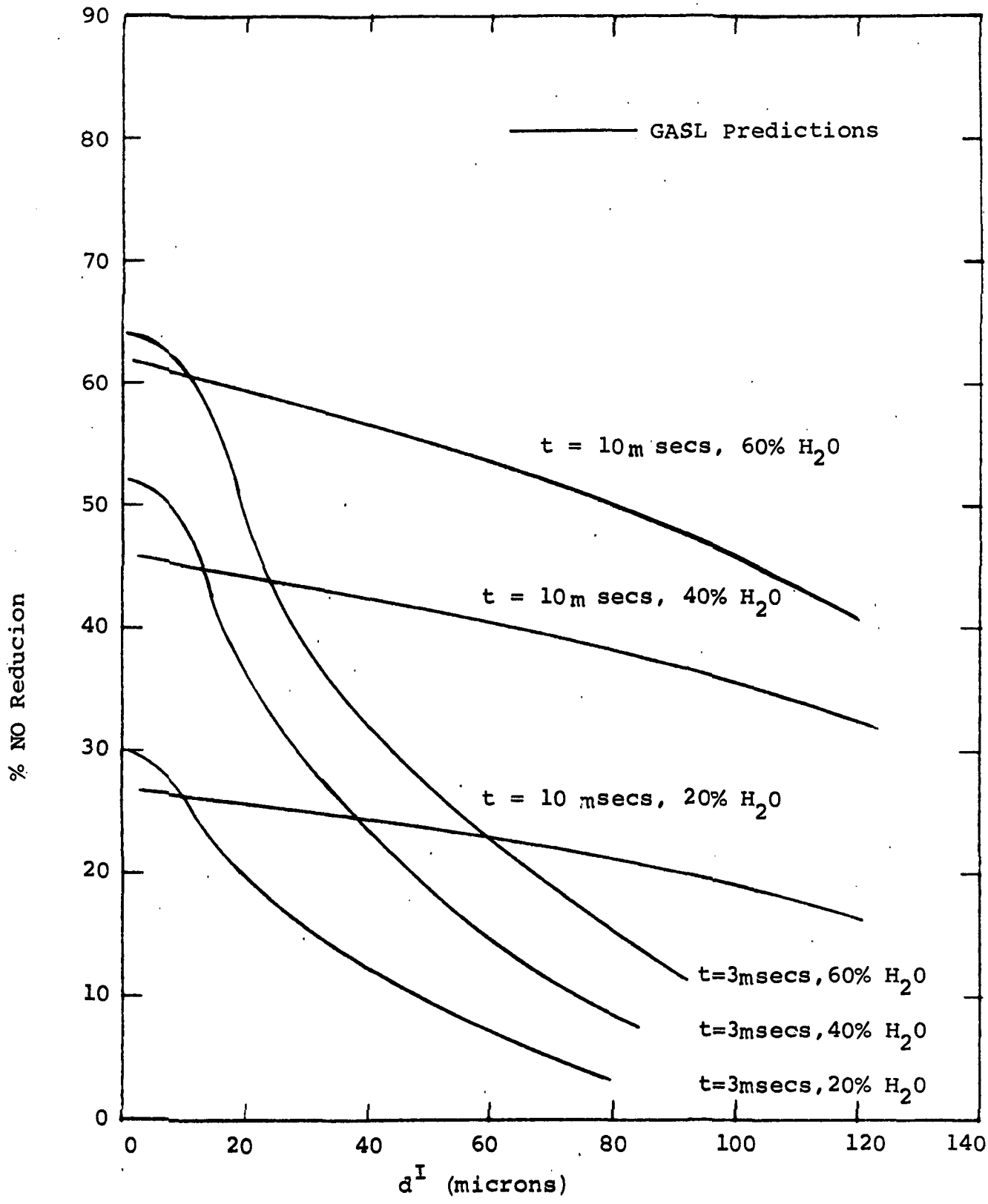


FIGURE 13 - NO REDUCTION AS A FUNCTION OF INITIAL WATER DROPLET DIAMETER FOR VARIOUS RESIDENCE TIMES AND WATER TO FUEL MASS RATIOS

## APPENDIX A

## FINITE-DIFFERENCE FORM OF GOVERNING EQUATIONS

The governing partial differential equations describing the conservation of mass, momentum, and energy within the flow field and along the axis can be readily put in an explicit finite-difference form. A backward-difference scheme is employed for the axial derivatives and a central-difference scheme for the radial derivatives.

Consider the flow field divided into a grid in $\psi$, x coordinates. Then the derivatives of an independent variable, say F, will be evaluated by

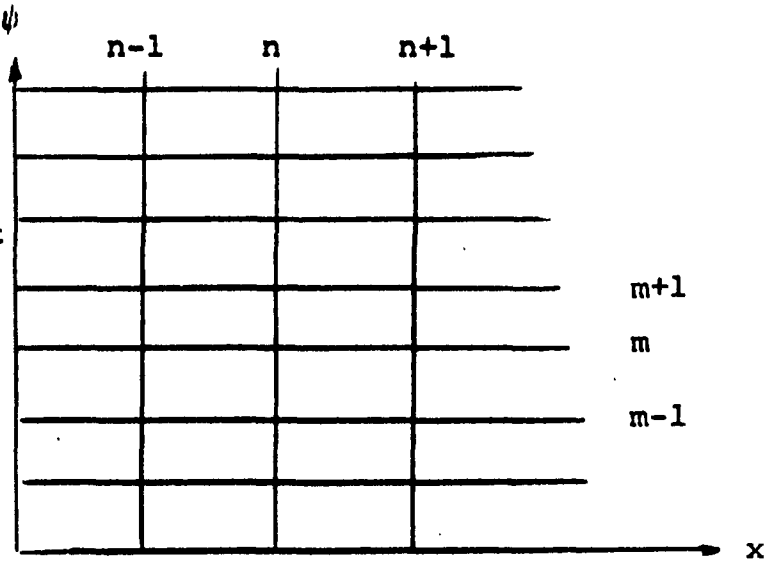


$$(\partial F/\partial x)_{n+1,m} = \frac{F_{n+1,m} - F_{n,m}}{\Delta x} = \frac{\Delta(F)_{n+1,m}}{\Delta x} \qquad \text{(A-1)}$$

$$\left(\frac{\partial F}{\partial \psi}\right)_{n,m} = \frac{F_{n,m+1} - F_{n,m-1}}{2\Delta\psi} = \frac{\Phi(F)_{n,m}}{\Delta\psi} \qquad \text{(A-2)}$$

$$\left[\frac{\partial}{\partial \psi}\left(a\,\frac{\partial F}{\partial \psi}\right)\right]_{n,m} = \frac{a_{n,m+\frac{1}{2}}(F_{n,m+1} - F_{n,m}) + a_{n,m-\frac{1}{2}}(F_{n,m-1} - F_{n,m})}{(\Delta\psi)^2}$$

$$= \Psi(a_{n,m}\langle F\rangle_{n,m}) \qquad \text{(A-3)}$$

where

$$a_{n,m\pm\frac{1}{2}} = (a_{n,m} + a_{n,m\pm1})/2 \qquad \text{(A-4)}$$

The m+1-ordered derivatives required for the equations along the axis are put into the form

$$\left(\frac{\partial^{m+1} F}{\partial \psi^{m+1}}\right)_{n,m} = \frac{F_{n,m+1} - 2M\, F_{n,m} + F_{n,m-1}}{(2-M)\ (\Delta\psi)^{m+1}} \tag{A-5}$$

Accordingly, using the formalism as described by the above equations, we have

$$\Delta(\alpha^i)_{n+1,m} = \Delta x \left\{ \frac{(\dot{w}_g)^i}{\rho u} + \frac{\Sigma(\dot{w}_p)^{ij}}{\rho u} \right\}_{n,m} + \frac{\Delta x}{\psi^M (\Delta\psi)^2} \cdot$$

$$\Psi \left\{ \left[ (A)\ \left(\frac{Le}{Pr}\right)_g\ (1-J_{D_i}) \right]_{n,m} <\alpha^i>_{n,m} \right\} \tag{A-6}$$

$$\Delta(\beta^j)_{n+1,m} = \Delta x \left\{ \frac{(\dot{w}_p)^j}{\rho u} \right\}_{n,m} + \frac{\Delta x}{\psi^M (\Delta\psi)^2} \cdot$$

$$\Psi \left\{ \left[ (A)\ \left(\frac{Le}{Pr}\right)_g\ \Theta_j\ (1-J_{D_j}) \right]_{n,m} <\beta^j>_{n,m} \right\} \tag{A-7}$$

$$(\Delta u)_{n+1,m} = \Delta x \left\{ \left(\frac{dr}{dx}\right)_{n+1,m} \left(\frac{\Gamma^2}{r^3 u}\right)_{n,m} - \left(\frac{dP}{dx}\right)_{n+1,m} \left(\frac{1}{\rho u}\right)_{n,m} \right\} + \frac{\Delta x}{\psi^M (\Delta\psi)^2} \cdot$$

$$\Psi \left\{ \left[ (A)\ J_m^{(x)} \right]_{n,m} <u>_{n,m} \right\} \tag{A-8}$$

$$(\Delta\Gamma)_{n+1,m} = \frac{\Delta x}{\psi^M \Delta\psi} \Psi \left\{ \left[ A\ \tilde{\mu}\ J_M^{(\theta)} \right] <\Gamma>_{n,m} \right\}_{n,m} - \frac{\Delta x}{\psi^M \Delta\psi} \Phi \left\{ \Gamma\ \tilde{\mu}^{(rx)} \right\}_{n,m} \tag{A-9}$$

$$(\Delta H)_{n+1,m} = \frac{\Delta x}{\psi^{M}\Delta\psi^{2}}\left\{\Psi\left\{\left[\frac{AJ_T}{P_r}\right]_{n,m}\langle H\rangle_{n,m}\right\} + \Psi\left\{\sum_i\left[\frac{A(L_e-1)}{P_r}\right]_{n,m} h_i\langle\alpha^i\rangle\right\}\right.$$

$$+ \Psi\left\{\sum_j\left[\frac{A(L_e-1)}{P_r}\right]_{n,m}\bar{\theta}_j h_j\langle\beta_j\rangle_{n,m}\right\}$$

$$+ \Psi\left\{\left[A(\alpha_g(\tilde{\mu}_g-1) - \sum_j \beta_j\delta_j\tilde{\mu}_j/\tilde{\mu}\right)\right]_{n,m}\langle q^2/2\rangle\right\}$$

$$\left.+ \Psi\left\{\left[A(\alpha_g(\tilde{\mu}_g-1) - \sum_j \beta_j\sigma_j\tilde{\mu}_j/\tilde{\mu}_g\right)\right]_{n,m}\langle w^2/2\rangle_{n,m}\right\}\right\}$$

$$- \frac{\Delta x}{\psi^{M}\Delta\psi}\left\{\Phi\left\{A\frac{J_D^{(g)}h_g\alpha_g}{S_c}\right\}_{n,m} + \Phi\left\{A\frac{J_D^{(p)}}{S_c}\sum\theta_j h_j\beta_j\right\}_{n,m}\right.$$

$$\left.+ \Phi\left\{A\mu^{(rx)}J_M^{(\theta)}\tilde{\mu}\,w^2\right\}_{n,m}\right\} \qquad \text{(A-10)}$$

The radial momentum, i.e.,

$$\partial p/\partial\psi = \psi^{M}\Gamma^{2}/ur^{4} \qquad \text{(A-11)}$$

can be obtained by simple quadrature and the quantity A in the above equations is defined as

$$A \equiv r^{2N}\mu_g^{(rx)}\rho u/\psi^{M} \qquad \text{(A-12)}$$

APPENDIX B

## RECIRCULATION ZONE ANALYSIS

The turbine combustor flow field involves recirculation zones and these regions would in general require an elliptic formulation to describe the associated nonuniformities and the upstream transmission of information. In the limit of intense backmixing, such imbedded zones will tend toward homogeneity and the state of flow can be characterized by a stirred-reactor analysis. The utility of a stirred-reactor model extends beyond just representing the imbedded recirculation zones. In certain cases of practical interest the entire primary zone can be a well mixed region and the stirred-reactor model is all that is needed to provide the state of flow in the entire primary zone. Of course, as a module, it will serve to indicate the relative importance of residence time, pressure and fuel/air ratio upon flame stability, (blow out), combustion efficiency, and pollutant emissions when the flow is well back mixed.

The describing equations are written for a zone having a specified volume, V, and are given as follows:

Global Conservation of Mass:

$$\dot{m} = \text{constant} = \sum_k \dot{m}_k^I = \sum_k \dot{m}_k^o \qquad \text{(B-1)}$$

where k is the $k^{th}$ component and includes i gas-phase species, and j droplet types. A droplet type (or class) is defined by its composition (fuel, water, etc.) and its size. The superscripts I and o refer to inflow and outflow, respectively.

Conservation of Energy:

$$h = h^I + \dot{Q}/\dot{m} \qquad \text{(B-2)}$$

where $\dot{Q}$ is the net rate of external heat addition to the reactor and the inflow of enthalpy is written to allow each component to enter the reactor with an arbitrary temperature. In particular,

$$h = \sum_i \alpha_i h_i(T) + \sum_j \alpha_j h_j(T_j) \quad , \tag{B-3}$$

and

$$h^I = \sum_i \alpha_i^I h_i(T_i^I) + \sum_j \alpha_j^I h_j(T_j^I) \tag{B-4}$$

where

$T$ = Local gas-phase temperature

$T_j$ = Local $j^{th}$ droplet temperature

$T_i^I$ = Injection temperature of the $i^{th}$ gas-phase specie

$T_j^I$ = Injection temperature of the $j^{th}$ droplet

To complete the specification of the thermal field some constraint governing the conservation of droplet energy is required. For the present it will be assumed that each droplet type is at its respective boiling-point temperature, i.e., $T_j = T_{j\ \text{Boiling Point}}$.

Conservation of Species:

The conservation of species k requires that its net outflow be equal to the rate of production due to chemical and phase transition processes. Formally, this principle gives k equations of the form:

$$\alpha_k = \alpha_k^I + \frac{V}{\dot{m}} [\hat{W}_k^G + \hat{W}_k^P] \tag{B-5}$$

where superscripts G and P refer to homogeneous gas-phase and dropwise production rates, respectively. The volumatric production rates are given as follows:

Homogeneous Gas Phase Reactions:

$$\hat{W}_i^G = W_i \sum_{p=1}^{R} (\nu''_{ip} - \nu'_{ip}) k_{f_p} \rho^{m_p} \prod_{i=1}^{N} \left(\frac{\alpha_i}{W_i}\right)^{\nu'_{ip}} \left[1 - \frac{\rho^{N_p}}{k_{c,p}} \prod_{i=1}^{N} \left(\frac{\alpha_i}{W_i}\right)^{\nu''_{ip} - \nu'_{ip}}\right] .$$

where

$$m_p = \sum_i^N \nu'_{ip} \quad ; \quad N_p = \sum_i^N (\nu''_{ip} - \nu'_{ip}) \tag{B-6}$$

for a chemical system containing N gas-phase species entering into R elementary reversible reactions given by:

$$\sum_{i=1}^{N} \nu'_{ip} M_i \underset{k_{b_p}}{\overset{k_{f_p}}{\rightleftharpoons}} \sum_{i=1}^{N} \nu''_{ip} M_i \quad , \quad p = \quad , \quad \ldots R \tag{B-7}$$

Dropwise Combustion and Evaporation:

For now, the droplet types will be specialized to fuel and water. Two limiting modes of consumption will be considered for the fuel droplet: (1) diffusion-controlled combustion and (2) evaporation only. In both cases a detailed homogeneous gas phase kinetics mechanism will be in effect. Of course, for the water only evaporation is relevant.

Fuel:

The two reactions considered are:

$$1. \quad C_nH_m + (n + \frac{m}{4}) O_2 - nCO_2 + \frac{m}{2} H_2O \tag{B-8}$$

$$2. \quad (C_nH_m)_{Liquid} - (C_nH_m)_{gas} \tag{B-9}$$

In both cases, the rate of consumption of the liquid fuel is given by diffusion controlled theory; viz:

$$(\hat{W}_{C_nH_m})^P = - 3/2 \rho d_{C_nH_m} \left( \frac{c^I}{d^{I3}_{C_nH_m}} \right) \lambda_{C_nH_m} \tag{B-10}$$

where

$$d^3_{C_nH_m} = d^{I^3}_{C_nH_m} \frac{\alpha_{C_nH_m\ell}}{\alpha^{I}_{C_nH_m\ell}} \tag{B-11}$$

and d is the droplet diameter. In addition,

$$\lambda_{C_nH_m} = 8\left(\frac{k}{C_p\delta}\right)_{C_nH_m} \ell n\ (1+B_{C_nH_m}) \tag{B-12}$$

where

$$B_{C_nH_m} = \frac{A(Y^{\circ}_{O_2})_g \left(\frac{\bar{H}}{\bar{N}}\right)_{C_nH_m} + C_{p_{C_nH_m}}(T-T^{B.P.}_{C_nH_m})}{Q_{C_nH_m}} \tag{B-13}$$

and k and $C_p$ are the thermal conductivity and specific heat of the vapor, respectively; $\bar{H}$ is the heat of combustion, $\bar{N}$ is the stoichiometric O/F ratio, $\delta$ is the droplet density and Q is the latent heat of vaporization.

Now, <u>for A = 1</u> we have:

$$(\dot{W}_{O_2})^P = \frac{(n+\frac{m}{4})\cdot W_{O2}}{nW_C+mW_H}(\dot{W}_{C_nH_m})^P \tag{B-14}$$

$$(\dot{W}_{C_{O2}})^P = -\frac{nW_{CO2}}{nW_C+mW_H}(\dot{W}_{C_nH_m})^P \tag{B-15}$$

$$(\dot{W}_{H_2O})^P_{gas} = -\frac{\frac{m}{2}W_{H_2O}}{nW_C+mW_H}(\dot{W}_{C_nH_M})^P - (\dot{W}_{H_2O})^P \tag{B-16}$$

and for A = 0:

$$(\dot{W}_{C_nH_m\,gas})^P = -(\dot{W}_{C_nH_m})^P \qquad \text{(B-17)}$$

In addition,

$$(Y_{O_2})_g = \frac{\alpha_{O_2}}{\sum_i \alpha_i}, \quad i = \text{all gases} \qquad \text{(B-18)}$$

Water - Here the reaction is:

$$(H_2O)_\ell \rightarrow (H_2O)_g \qquad \text{(B-19)}$$

where

$$(\dot{W}_{H_2O})^P = -3/2\ \rho\ d_{H_2O}\ \left(\frac{\alpha}{d^3}\right)^I_{H_2O}\ \lambda_{H_2O} \qquad \text{(B-20)}$$

and

$$\lambda_{H_2O} = 8\left(\frac{k}{C_p\delta}\right)_{H_2O} \ln(1+B_{H_2O}) \qquad \text{(B-21)}$$

with

$$B_{H_2O} = \frac{C_{p_{H_2O}}(T-T^{B.P.}_{H_2O})}{Q_{H_2O}} \qquad \text{(B-22)}$$

and

$$d^3_{H_2O} = d^{I^3}_{H_2O}\ \frac{\alpha_{H_2O\ell}}{\alpha^I_{H_2O\ell}} \qquad \text{(B-23)}$$

State:

$$\rho = \frac{P}{RT \sum_i \frac{\alpha_i}{W_i}} \quad , \quad i = \text{all gases ...} \tag{B-24}$$

where $\rho$ is the mixture density and T is the gas-phase temperature.

Although there exist more or less standard techniques for the solution of such algebraic equations, the iterations required and the tracking and exclusion of the non-physical solutions renders such an approach extremely cumbersome. An alternative approach is that of seeking the asymptotic (steady state) solution to a transient problem wherein the "boundary conditions" are held fixed at the desired steady state values. This leads to a "marching on" problem which eliminates the difficulties encountered in the solution of the algebraic equations. In essence, our approach involves the use of the non-steady form of the species conservation equations, viz:

$$\frac{d\alpha_k}{dt} = \frac{\dot{m}}{\rho V}(\alpha_k^I - \alpha_k) + \left(\frac{\dot{W}_k}{\rho}\right)^G + \left(\frac{\dot{W}_k}{\rho}\right)^P \tag{B-25}$$

where t is the time variable of significance only during the transient period. Thus, Eq. (B-25) is identical to Eq. (B-5) when:

$$\frac{d\alpha_k}{dt} \to 0. \tag{B-26}$$

The remaining working equations retain their steady state form. To initiate a calculation requires the specification of the $\alpha_k$'s at t = o. We start with the equilibrium state although this "initial" composition may be chosen arbitrarily.

NASA, Lewis Research Center
Contract NASw-2235 - GASL Project 5865

---

DISTRIBUTION LIST

Reproducible + 2 cys. to:
NASA Scientific & Technical Information Facility
P. O. Box 33
College Park, Maryland 20740

4 cys. to:
NASA Headquarters
Washington, D.C. 20546
Attn: Code: RAA

1 cy. each to:
NASA Headquarters
Washington, D. C. 20546
Attn: Code: KT - New Technology Representative

Naval Air Propulsion Test Center
Bldg. 600
Philadelphia Naval Base
Philadelphia, PA 19112

Environmental Protection Agency
5 Research Drive
Ann Arbor, MI 48103
Attn: Mr. George Kittredge (1)
Mr. William Mirsky (1)

Federal Aviation Administration
800 Independence Avenue, S.W.
Washington, D. C. 20590
Attn: Mr. William Westfield

Commanding Officer, Eustice Directorate
U.S.Army Air Mobility Research & Development Lab.
Ft. Eustice, VA 23604
Attn: L. Bell - SAVDL-EU-PP

*DISTRIBUTION LIST - Cont'd.

1 cy. each to:

NASA-Lewis Research Center
21000 Brookpark Road
Cleveland, Ohio 44135

Attn: Mr. Richard Rudey, M.S. 60-6

Attn: Mr. Jack Grobman, M.S.60-6

Attn: Dr. Cecil J. Marek, M.S.60-4

Attn: Mr. Paul Wieber, M.S.7-1

Attn: Dr. Richard Brokaw, M.S.6-1

Attn: Mr. Robert Jones, M.S.60-6

(as of 11/71) Attn: Dr. David Anderson (Project Manager) M.S.60-4

" " " Attn: Dr. Howard Childs, Chief
Air Breathing Engine Division (Technical Representative)

" " " Attn: Mr. Leonard W. Schopen (Contracting Officer) M.S.77-3